GPS/INS/G Sensors/Yaw Rate Sensor/Wheel Speed Sensors Integrated Vehicular Positioning System

Jianchen Gao
Position, Location And Navigation (PLAN) Group
Department of Geomatics Engineering
Schulich School of Engineering
University of Calgary

BIOGRAPHY

Jianchen Gao is a PhD candidate in the Department of Geomatics Engineering at the University of Calgary. He received a PhD degree in Mechatronics at the Beijing Institute of Technology, an MSc in Automatic Control at the Beijing Institute of Technology, and a BSc in Automatic Control at the Hebei University of Science and Technology. His current research area is in GPS/INS/On-board vehicle sensor integrated positioning and navigation systems.

ABSTRACT

This paper discusses in detail the integration strategy and algorithms for the integration of GPS, a tactical grade HG1700 IMU, G sensors which measure horizontal specific force, a yaw rate sensor and wheel speed sensors. Using a tight coupling strategy, the dynamic and measurement models of a centralized Kalman filter are developed. The research investigates the use of non-holonomic constraints which are typically used in vehicle positioning applications, and the limitations of these constraints are reduced through use of the auxiliary sensors. An algorithm for on-line tuning of the velocity variance for velocity updates is investigated. GPS data collected in the field is used to compare the performance of four integration strategies, namely a GPS/INS integrated system, a GPS/INS/G sensors/Yaw rate sensor/Wheel speed sensor system with two non-holonomic constraints, a GPS/INS/G sensors/Yaw rate sensor/Wheel speed sensor system with the replacement of the lateral constraint by the estimated lateral velocity, and a GPS/INS/G sensors/Yaw rate sensor/Wheel speed sensor system with the removal of the lateral constraint by decomposing the wheel speed sensor measurement with the side slip angle.

INTRODUCTION

Due to their complementary features, GPS/INS integrated systems have been widely used for vehicular positioning and navigation. To bridge gaps during GPS outages, many auxiliary sensors have been used to provide further external aiding to reduce the INS error growth. In the vehicular positioning systems, the typical auxiliary sensors may include compasses, inclinometers, tilt meters (Harvey, 1998), odometers (Stephen, 2000), or wheel speed sensors, to name a few. Among these, the wheel speed sensors are fundamental components of an ABS which is standard equipment on nearly all vehicles (Hay, 2005). Therefore the integration of the wheel speed senor or odometer with GPS/INS has been extensively studied (Kubo et al., 1999; Gao et al., 2006). Since the wheel speed sensor only measures velocity in the forward direction, most of the previous research related to the integration of wheel speed sensor information with GPS/INS applies two non-holonomic constraints on the lateral and vertical directions. These non-holonomic constraints are effective only when the vehicle operates on a flat road and no side slip occurs (Brandt et al., 1998; Dissannayake et al., 2001). In practical use, however, the non-holonomic constraints are no longer valid when the vehicle runs on the off-road or on a bumpy road whereby a larger side slip angle appears. To alleviate the limitation of these constraints, one option is to detect the violation of the constraints and then replace them by other effective measurements.

In a land vehicular positioning system, the violation of the non-holonomic constraints is always accompanied by larger side slip angles. Side slip is a very complicated phenomenon whereby it often occurs instantaneously, and it is not easily modeled and estimated. Sujit et al. (1997) used appropriate approximations and proper sensor placements to estimate tire side slip angles without reference to a dynamic model of the vehicle. Ray (1995)

developed a nonlinear state and tire force estimation algorithm to calculate the side slip angle indirectly. Anderson et al. (2004) explored a model-based Kalman filter with GPS velocity measurements to estimate side slip. However, its estimation accuracy relies heavily on the correctness of the model.

Based on the above analysis and the previous research, this paper incorporates G sensors (GL) (which measures the lateral and longitudinal specific forces) and a Yaw Rate Sensor (YRS) (which measures the angular rate with respect to the vertical direction) with the Wheel Speed Sensors (WSS) to compute the lateral velocity and the side slip angle, which can be used to detect violations of the non-holonomic constraints. By creating a relationship between different on-board vehicle sensors rather than working independently, the internal constraints between different sensors outperform the external constraints. Two possible ways are designed to alleviate the limitations of the non-holonomic constraints. The first is to use the computed lateral velocity to remove the lateral constraint. The second is to decompose the wheel speed sensor measurement into longitudinal and lateral velocities by the side slip angle, and the decomposed lateral velocity can also be used to replace the lateral constraint.

The G sensors, yaw rate sensor and wheel speed sensors are integrated with GPS/INS through a tight coupling strategy. Due to the installation error of the vehicle sensors, the bore sights of the GL/YRS, the WSS, as well as IMU, are not highly aligned. An on-line calibration algorithm was designed to estimate the misalignment angle between the IMU and the vehicle sensors. After updating the Kalman filter by GL/YRS and the WSS, the Kalman filter can estimate the error states of the misalignment angles between different frames, the WSS scale factor as well as the GL/YRS biases for more accurate computation of the lateral velocity and the side slip angle.

The required accuracy of this research is at the centimeter level so an HG1700 tactical grade IMU and GPS carrier phase measurements with resolved integer ambiguities are used. To evaluate the effects of different integration strategies and algorithms, GPS outages were simulated for an analysis of the horizontal positioning drift error with respect to four integration strategies, namely a GPS/INS integrated system, a GPS/INS/GL/YRS/WSS integrated system with two non-holonomic constraints for the WSS update, a GPS/INS/GL/YRS/WSS system with the replacement of the lateral constraints by the estimated lateral velocity, and a GPS/INS/GL/YRS/WSS system with the removal of the lateral constraints by decomposing the wheel speed sensor measurement with the side slip angle.

The paper first describes the location and coordinate frames of the vehicle sensors and the HG1700 IMU. Second, the integration strategy and algorithms are analyzed in detail. Then the field test is introduced, and the results are shown and compared. Conclusions are given at the end of the paper.

THE LOCATION AND COORDINATE FRAME DEFINITIONS OF VEHICLE SENSORS AND IMU

Figure 1 describes the approximate location of the IMU and the on-board vehicle sensors. Two rear and two front wheel speed sensors are attached to the wheels. The tactical grade HG1700 IMU is mounted on the top of the vehicle and the GL/YRS are placed on the chassis of the vehicle to constitute a two dimensional automotive-grade IMU.

Figure 1 defines the coordinate frames: the IMU body frame (b-frame), the vehicle body frame (v-frame). For the IMU body frame, the X-axis points towards the right direction, the Y-axis points toward the forward direction, and the Z-axis is orthogonal to the X and Y axes to complete a right-handed system. The vehicle frame is attached to the center of gravity. Its X-axis points toward the right side of the vehicle, the Y-axis points towards the forward direction of the vehicle and the Z-axis is orthogonal to the X and Y axes to complete a right handed frame. Being similar to the IMU body frame, the two dimensional GL/YRS also has its own body frame (GY body frame). Its X-axis points towards the right side of the moving platform, and the Y-axis points towards the forward direction of the moving platform.

In an ideal case, the b, v and GY frames are aligned. However, due to installation "errors", the misaligned angles between the different sensor frames will result in some errors when the position or velocity is transformed from one frame to another without taking into account the misalignment angles. To be precise, the misalignment angles of the v and GY frames with respect to the b frame are estimated in this research. With the estimated misalignment angles of the v frame or the GY frame with reference to the b frame, the direction cosine matrices are calculated by Equations (1) or (2).

$$R_b^v = R_3(\gamma^{b-v}) \cdot R_1(\alpha^{b-v}) \cdot R_2(\beta^{b-v}) \qquad (1)$$

where α^{b-v}, β^{b-v}, γ^{b-v} are the misalignment angles between the b and v frames with respect to the X, Y and Z axes, respectively.

$$R_b^{GY} = R_3(\gamma^{b-GY}) \cdot R_1(\alpha^{b-GY}) \cdot R_2(\beta^{b-GY}) \qquad (2)$$

where α^{b-GY}, β^{b-GY}, γ^{b-GY} are the misalignment angles

between the b and GY frames with respect to the X, Y and Z axes, respectively.

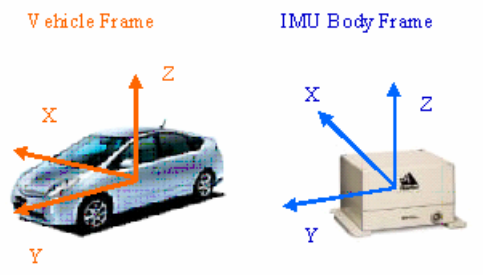

Figure 1: IMU and On-Board Vehicle Sensor Coordinate Frame Definitions

INTEGRATION STRATEGY AND ALGORITHMS

Information from GPS, the HG1700 tactical grade IMU, and the on-board sensors are integrated using a tight coupling strategy as per Figure 2. GPS measurements include the double difference Doppler, pseudorange and the carrier phase observables. The IMU mechanization equation is implemented in the ECEF frame (e frame) at 20 Hz. The centralized Kalman filter estimates the error states, such as the position, velocity, b to e frames misalignment angles, IMU gyro and accelerometer biases, to correct the IMU measurements and the mechanization equation outputs. When the WSS and the GL/YRS are integrated with GPS/INS, the error states of the misalignment angles of v or GY frame with reference to the b frame, the WSS scale factor, and the GL/YRS biases are augmented into the centralized Kalman filter. The WSS scale factor takes into account tire radius changes due to different load and driving conditions. The WSS provides absolute velocity information to update the centralized Kalman filter. Similarly, other velocity information can also be derived from the GL/YRS to conduct the update.

In Figure 2, the relationship between the centralized Kalman filter and the velocity update (either from the WSS or the GL/YRS) are bidirectional. In one way, the velocity update can function as an external aid to limit the INS error drift during GPS outages. It has been verified by Gao et al. (2006) that the WSS with two non-holonomic constraints can significantly improve the positioning accuracy when the non-holonomic constraints are not violated. The quality of the automotive grade GL/YRS is much lower than the tactical grade IMU, and the benefits gained from the GL/YRS during GPS outages are somewhat limited. In the other direction, the estimated error states can correct the vehicle sensor measurements and the misalignment angles. More specifically, the GL/YRS raw measurements can be corrected by the estimated biases after the GL/YRS velocity update to generate a more accurate lateral velocity. This provides the possibility of incorporating the GL/YRS with WSS to detect and alleviate any violations of the non-holonomic constraints in the WSS.

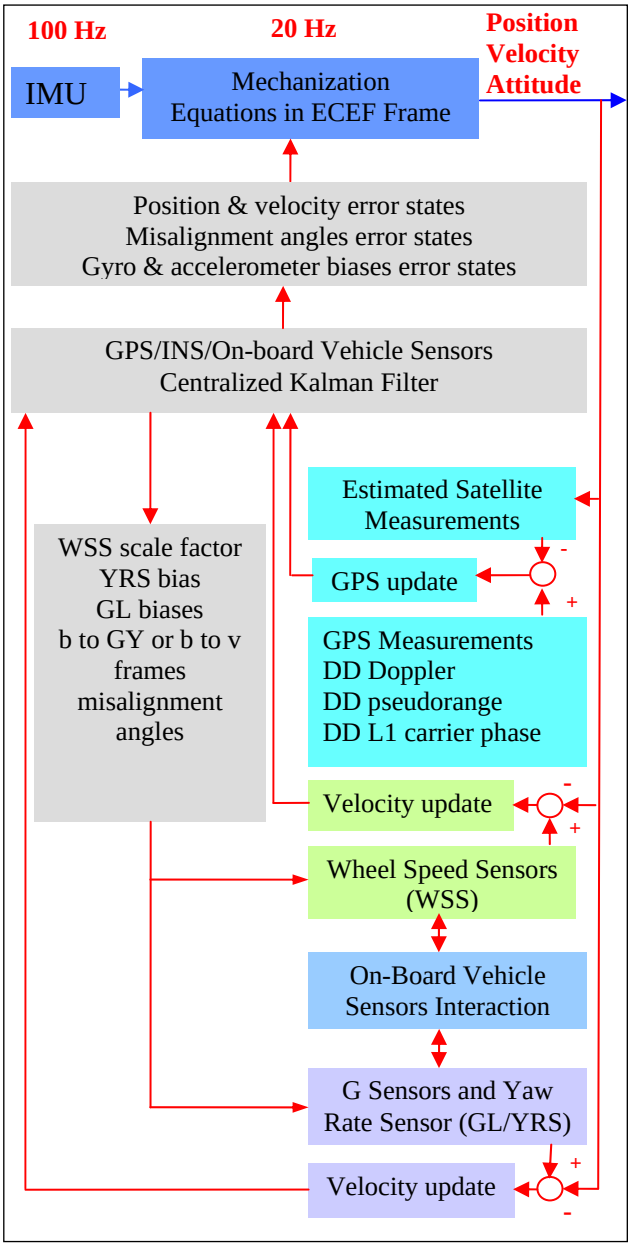

Figure 2: Schematic of the Integration Strategy

Figure 3 describes the interactive relationship between the WSS and the GL/YRS. The WSS measures the velocity in Y-direction of the vehicle frame. It is a natural way to apply non-holonomic constraints in the X and Z directions of the vehicle frame. The WSS velocity update can be carried out either in the v frame or in the e frame by an appropriate velocity transformation with the direction cosine matrix. In this research, the WSS velocity update is carried out in the v frame. Incorporating GL/YRS with the

WSS can provide the lateral velocity or the side slip angle information to alleviate the violation of the non-holonomic constraints. WSS increase the accuracy of the longitudinal initial velocity to GL/YRS. The GL/YRS performs a velocity update in the GY frame by calculating the velocity from the GL/YRS measurements corrected by the estimated error states of GL/YRS biases. With the lateral velocity, the WSS non-holonomic constraint in the lateral direction can be removed. Alternatively, the side slip angle can be calculated from the lateral and longitudinal velocities. The WSS measurement can be decomposed into lateral and longitudinal directions using the side slip angle. From this point of view, the GPS/INS/GL/YRS/WSS integration strategy can be implemented in three ways.

1. The GL/YRS and WSS update the centralized Kalman filter sequentially and two non-holonomic constraints are used for the WSS update.

2. The GL/YRS and WSS update the centralized Kalman filter sequentially and the WSS makes use of the lateral velocity calculated from the GL/YRS to replace the non-holonomic constraint in the lateral direction.

3. The GL/YRS and WSS update the centralized Kalman filter sequentially and the side slip angle is calculated from the GL/YRS lateral and longitudinal velocities. Decomposing the WSS measurement by the side slip angle into longitudinal and lateral directions can also remove the lateral constraint.

The development of the integration algorithms includes the derivations of the dynamic and measurement equations used in the Kalman filter, the equation of motion for GL/YRS, the relationship between GL/YRS and WSS, as well as the on-line tuning of the velocity variances for the velocity update.

The error states related to the on-board vehicle sensors are augmented into the GPS/INS centralized Kalman filter. The dynamic matrix is given in Equation (3) on the basis of GPS/INS system developed by Petovello (2003). It implies that the bias states are modeled as first-order Gauss-Markov processes. The scale factor of the wheel speed sensors and the misalignment angles between the b and v frames, as well as those between the b and GY frames, are modeled as random constants.

As shown in Figure 4, the G sensors GL1 and GL2 are placed with a 45 degree offset with respect to the GY frame. The G sensors are actually two-dimensional accelerometers, and the GPS/INS integrated system is three dimensional. When the G sensors are integrated with GPS/INS, the non-holonomic constraint in the vertical direction is applied by assuming the specific force in the vertical direction is always zero.

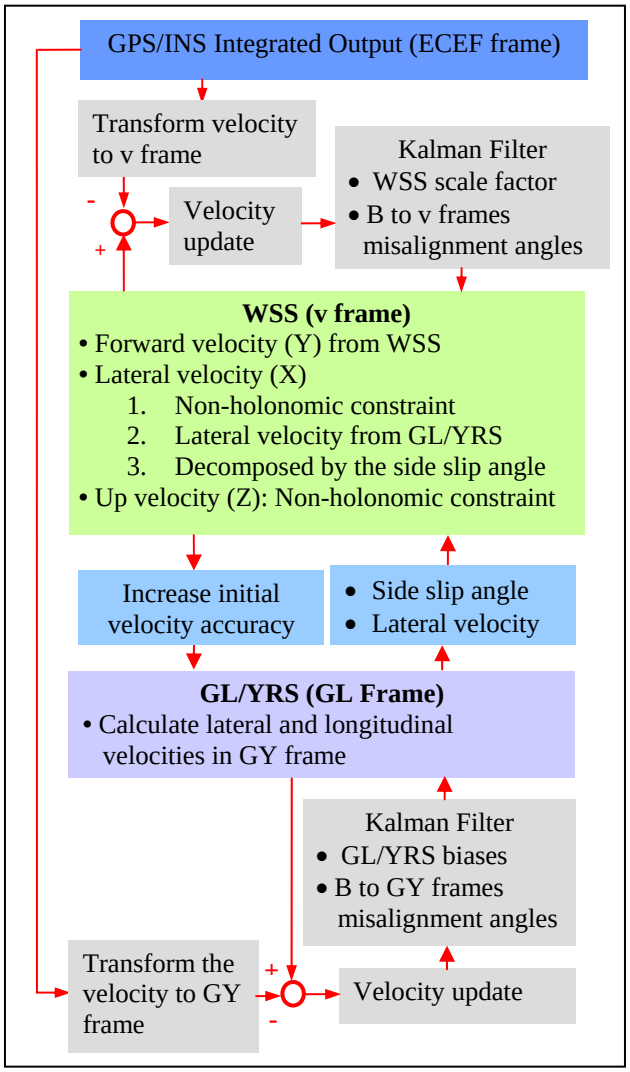

Figure 3: Interactive Relationship between the Wheel Speed Sensors, G sensors and Yaw Rate Sensor

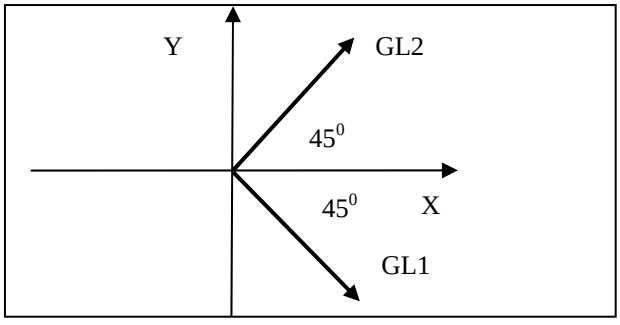

Figure 4: The placement of GL1 and GL2 sensors

$$
\begin{bmatrix} \dot{\delta r}^e \\ \dot{\delta v}^e \\ \dot{\varepsilon}^{b-e} \\ \dot{\delta b}^b \\ \dot{\delta d}^b \\ \dot{\Delta \nabla N} \\ \dot{\delta S} \\ \dot{\varepsilon}_{b-v} \\ \dot{\delta d}_{Yaw} \\ \dot{\delta b}_{GL} \\ \dot{\varepsilon}_{b-GY} \end{bmatrix} =
\begin{bmatrix}
0 & I & 0 & 0 & 0 & , \\
N^e & -2\Omega_{ie}^e & -F^e & R_b^e & 0 & , \\
0 & 0 & -\Omega_{ie}^e & 0 & R_b^e & , \\
0 & 0 & 0 & -diag(\alpha_i) & 0 & , \\
0 & 0 & 0 & 0 & -diag(\beta_i) & , \\
0 & 0 & 0 & 0 & 0 & , \\
0 & 0 & 0 & 0 & 0 & , \\
0 & 0 & 0 & 0 & 0 & , \\
0 & 0 & 0 & 0 & 0 & , \\
0 & 0 & 0 & 0 & 0 & , \\
0 & 0 & 0 & 0 & 0 & ,
\end{bmatrix}
$$

$$
\begin{bmatrix}
0 & 0 & 0 & 0 & 0 & 0 \\
0 & 0 & 0 & 0 & 0 & 0 \\
0 & 0 & 0 & 0 & 0 & 0 \\
0 & 0 & 0 & 0 & 0 & 0 \\
0 & 0 & 0 & 0 & 0 & 0 \\
0 & 0 & 0 & 0 & 0 & 0 \\
0 & 0 & 0 & 0 & 0 & 0 \\
0 & 0 & 0 & 0 & 0 & 0 \\
0 & 0 & 0 & -\beta_{Yaw} & 0 & 0 \\
0 & 0 & 0 & 0 & -\beta_{GL} & 0 \\
0 & 0 & 0 & 0 & 0 & 0
\end{bmatrix}
\cdot
\begin{bmatrix} \delta r^e \\ \delta v^e \\ \varepsilon^{b-e} \\ \delta b^b \\ \delta d^b \\ \Delta \nabla N \\ \delta S \\ \varepsilon_{b-v} \\ \delta d_{Yaw} \\ \delta b_{GL} \\ \varepsilon_{b-GY} \end{bmatrix}
$$

$$
+
\begin{bmatrix}
0 & 0 & 0 & 0 & 0 & 0 \\
R_b^e & 0 & 0 & 0 & 0 & 0 \\
0 & R_b^e & 0 & 0 & 0 & 0 \\
0 & 0 & I & 0 & 0 & 0 \\
0 & 0 & 0 & I & 0 & 0 \\
0 & 0 & 0 & 0 & 0 & 0 \\
0 & 0 & 0 & 0 & 0 & 0 \\
0 & 0 & 0 & 0 & 0 & 0 \\
0 & 0 & 0 & 0 & 1 & 0 \\
0 & 0 & 0 & 0 & 0 & 1 \\
0 & 0 & 0 & 0 & 0 & 0
\end{bmatrix}
\cdot
\begin{bmatrix} w_f \\ w_w \\ w_b \\ w_d \\ w_{Yaw} \\ w_{GL} \end{bmatrix}
\qquad (3)
$$

$$
= F_{GPS/INS/GL/YRS/WSS} \cdot \delta x + G \cdot w
$$

where δr^e is the position error vector (3x1). δv^e is the velocity error vector (3x1). ε^{b-e} is the error vector of misalignment angles (3x1) between the b and e frames. δb^b is the error vector of the accelerometer biases (3x1). δd^b is the error vector of gyro biases (3x1). $\Delta \nabla N$ is the double differenced carrier phase ambiguities. δS is the error of WSS scale factor. ε^{b-v} is the error vector of misalignment angles between the b and v frames. $\varepsilon^{b-v} = \begin{bmatrix} \delta\alpha^{b-v} & \delta\beta^{b-v} & \delta\gamma^{b-v} \end{bmatrix}$. ε^{b-GY} is the error vector of misalignment angles between the b and GY frames. $\varepsilon^{b-GY} = \begin{bmatrix} \delta\alpha^{b-GY} & \delta\beta^{b-GY} & \delta\gamma^{b-GY} \end{bmatrix}$. δd_{Yaw} is the error of yaw rate sensor bias (1x1). δb_{GL} is the error vector of the G sensor biases (2x1). $diag(\alpha_i)$ is a diagonal matrix of time constants for the accelerometer bias models. $diag(\beta_i)$ is a diagonal matrix of time constants for the gyro bias models. β_{Yaw} (1x1) and β_{GL} (2x1) are the time constant for the YRS and GL biases models respectively. R_b^e is the direction cosine matrix between the b and e frames. F^e is the skew-symmetric matrix of specific force in the e frame. N^e is the tensor of the gravity gradients. Ω_{ie}^e is the skew-symmetric matrix of the Earth rotation rate with respect to the e frame. w_f and w_w are the accelerometer and gyro noises respectively. w_b, w_d, w_{Yaw} and w_{GL} are the driving noises for the accelerometer biases, the gyro biases, the YRS bias and GL biases respectively. $F_{GPS/INS/GL/YRS/WSS}$ is the dynamic matrix for the GPS/INS/GL/YRS/WSS integration strategy. δx is the error state. G is the shaping matrix, and w is the process noise.

The lateral and longitudinal specific forces can be derived from the GL1 and GL2 measurements shown by Equation (4).

$$
\begin{cases} f_x = (G_{L1} + G_{L2}) \cdot \cos(\pi/4) \\ f_y = (G_{L2} - G_{L1}) \cdot \cos(\pi/4) \\ f_z = 0 \end{cases} \qquad (4)
$$

where f_x, f_y, f_z are the specific forces in the lateral, longitudinal and vertical directions in the GY frame.

With the lateral and longitudinal specific forces, as well as the yaw rate sensor measurement, the equation of motion in the GY frame is shown in Equation (5) (Dissanayake et al. , 2001). It describes the relationship of the lateral, longitudinal and the vertical velocities with the specific forces and the yaw rate corrected by the estimated biases as well as gravity in GY frame. Since the non-holonomic constraint is applied in the vertical direction, the vertical velocity is only coupled with gravity.

$$
\begin{cases} \dot{V}_x^{GY} = (f_x - b_{GL1}) - V_y \cdot (r - d_{Yaw}) + g_x^{GY} \\ \dot{V}_y^{GY} = (f_y - b_{GL2}) + V_x \cdot (r - d_{Yaw}) + g_y^{GY} \\ \dot{V}_z^{GY} = g_z^{GY} \end{cases} \qquad (5)
$$

where γ is the yaw rate , $V_x^{GY}, V_y^{GY}, V_z^{GY}$ are the velocities in the X, Y and Z direction of the GY frame, and $g_x^{GY}, g_y^{GY}, g_z^{GY}$ are the gravity elements in the GY frame. b_{GL1}, b_{GL2} and d_{Yaw} are the biases of GL and YRS respectively.

The gravity vector in Equation (5) is derived from the gravity vector in the e frame by Equation (6).

$$g^{GY} = R_b^{GY} \cdot \left(R_b^e\right)^T \cdot g^e \quad (6)$$

where g^e is the gravity vector in the e frame. R_b^{GY} is the direction cosine matrix between the b and GY frames, and R_b^e is the direction cosine matrix between the b and e frames.

If assuming

$$M = \begin{bmatrix} 1 & 0 & 0 \\ 0 & 1 & 0 \\ 0 & 0 & 0 \end{bmatrix}, \quad f = \begin{bmatrix} f_x \\ f_y \\ 0 \end{bmatrix}, \quad J = \begin{bmatrix} 0 & -1 & 0 \\ 1 & 0 & 0 \\ 0 & 0 & 0 \end{bmatrix} \quad (7)$$

Equation (5) can be replaced by the state space vector in Equation (8) , which simplifies the mathematical analysis.

$$\dot{V}^{GY} = M \cdot \left(f - b_{GL}\right) + J \cdot V^{GY} \cdot \left(\gamma - d_{Yaw}\right) + g^{GY} \quad (8)$$

where V^{GY} is the velocity vector in the GY frame. f is the specific force vector in the GY frame. g^{GY} is the gravity vector in the GY frame. b_{GL} is the G sensor biases. M, J are the coefficients defined in Equation (7).

Only the two rear wheel speed sensors are considered as the front wheel speed sensors are correlated with the steering angle information which is not used here. Assuming no side slip, the velocity in the Y direction of the vehicle frame is given by averaging the two rear wheel speed sensor measurements in Equation (9).

$$v_{wss} = \left(V_{RL} + V_{RR}\right)/2 \quad (9)$$

where v_{wss} is the average of the rear wheel speed sensor measurements.

Using the Euler or trapezoid method (Jekeli, 2000), the velocity in the GY frame can be integrated from Equation (8). Figure 5 describes the geometric relationship between the WSS and GL/YRS. The velocity computed from the GL/YRS can be transformed into the v frame by Equation (10).

$$V_{GY}^v = R_b^v \cdot \left(R_b^{GY}\right)^T \cdot V^{GY} \quad (10)$$

where V_{GY}^v is the transformed velocity from the GY frame to the v frame.

Figure 6 shows the vehicle's bicycle model that contains the rear and front wheels side slip angles β_r and β_f as well as the steering angle σ_f . The rear wheel side slip angle can be calculated in Equation (11) from the transformed velocity in the lateral and longitudinal directions of the v frame shown in Equation (10) (Ray, 1995).

$$\beta_r = \tan^{-1}\left[\frac{(V_{GY}^v)_x - L_r \cdot \gamma}{(V_{GY}^v)_y}\right] \quad (11)$$

where β_r is the rear wheel side slip angle. L_r is the distance between the GL/YRS and WSS. $(V_{GY}^v)_x$ and $(V_{GY}^v)_y$ are the lateral and longitudinal elements of the transformed velocity between the b and GY frames respectively.

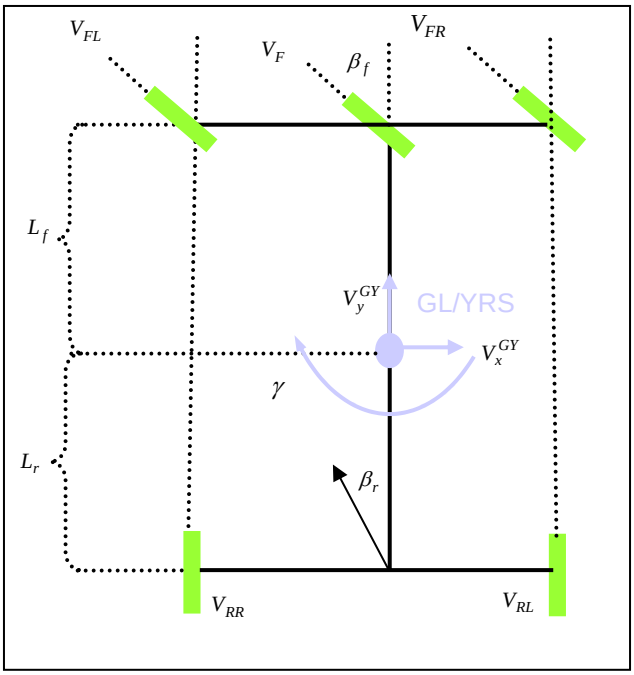

Figure 5: Geometric Relationship between the Wheel Speed Sensor, G sensors and Yaw Rate Sensor

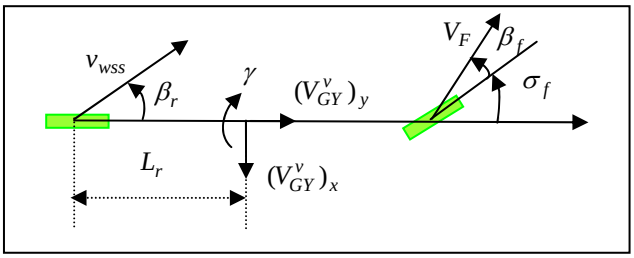

Figure 6: Bicycle Model that Contains Rear and Front Side Slip Angles

From the above analysis, three options are available to constitute the measurements for a WSS update.

Case I: Non-holonomic constraints are applied in the lateral and vertical directions. The velocity in the Y direction comes from the WSS measurement, as shown in Equation (12).

$$V_{WSS} = \begin{bmatrix} 0 \\ v_{WSS} \\ 0 \end{bmatrix} \quad (12)$$

Case II: The lateral element of the transformed velocity between GY and V frames is used to replace the lateral constraint, as shown in Equation (13).

$$V_{WSS} = \begin{bmatrix} \left(V_{GY}^{v}\right)_x \\ v_{wss} \\ 0 \end{bmatrix} \quad (13)$$

Case III: The WSS measurement is decomposed by the side slip angle into lateral and longitudinal velocities in the v frame. It is expressed in Equation (14).

$$V_{WSS} = \begin{bmatrix} v_{wss} \cdot \sin\beta_r \\ v_{wss} \cdot \cos\beta_r \\ 0 \end{bmatrix} \quad (14)$$

The measurement model for the Kalman filter is expressed by Equation (15).

$$Z = H \cdot \delta x + \omega_m \quad (15)$$

where H is the design matrix, ω_m is the measurement noise and Z is the measurement residual.

Based on Equation (8), the velocity can be calculated simply by Equation (16).

$$V^{GY} = V_0^{GY} + \left[M \cdot \left(f - b_{GL} \right) + J \cdot V_0^{GY} \cdot \left(\gamma - d_{Yaw} \right) + g^{GY} \right] \cdot \Delta t \quad (16)$$

where V_0^{GY} is the initial velocity that comes from integrated system, and Δt is the integration time interval. $\Delta t = 1\,s$ in this research.

To conduct the GL/YRS update in GY frame, the velocity in the integrated system is transformed into the GY frame, and the measurement equation is expressed by Equation (17).

$$V^{GY} = R_b^{GY} \cdot \left(R_b^e\right)^T \cdot v^e \quad (17)$$

where v^e is the velocity of the integrated system in the e frame.

The perturbation of the gravity vector in Equation (6) can be derived as shown in Equation (18).

$$\begin{aligned} \delta g^{GY} &= R_b^{GY} \cdot \left(R_b^e\right)^T \cdot N^e \cdot \delta r^e + R_b^{GY} \cdot \left(R_b^e\right)^T \cdot G^e \cdot \varepsilon^{b-e} \\ &\quad - G^{GY} \cdot \varepsilon^{b-GY} \end{aligned} \quad (18)$$

where N^e is the tensor of the gravity gradients. G^e is the skew-symmetric matrix of the gravity vector in the e frame, G^{GY} is the skew-symmetric matrix of the gravity vector in the GY frame.

The perturbation of the velocity in the GY frame is derived in Equation (19).

$$\begin{aligned} \delta V^{GY} &= \left(M \cdot \delta f + J \cdot V_0^{GY} \delta\gamma + \delta g^{GY} \right) \cdot \Delta t \\ &= M \cdot \Delta t \cdot \delta b_{GL} + J \cdot \Delta t \cdot \delta d_{Yaw} \\ &\quad + R_b^{GY} \cdot \left(R_b^e\right)^T \cdot N^e \cdot \Delta t \cdot \delta r^e \\ &\quad + R_b^{GY} \cdot \left(R_b^e\right)^T \cdot G^e \cdot \Delta t \cdot \varepsilon^{b-e} - G^{GY} \cdot \Delta t \cdot \varepsilon^{b-GY} \end{aligned} \quad (19)$$

The perturbation on the right hand side of Equation (17) are shown in Equation (20).

$$\begin{aligned} \delta\left(R_b^{GY} \cdot \left(R_b^e\right)^T \cdot v^e \right) &= R_b^{GY} \cdot \left(R_b^e\right)^T \cdot \delta v^e \\ &\quad + R_b^{GY} \cdot \left(R_b^e\right)^T \cdot V^E \cdot \varepsilon^{b-e} \\ &\quad - V^{GY} \cdot \varepsilon^{b-GY} \end{aligned} \quad (20)$$

where V^E is the skew-symmetric matrix of the integrated velocity in the e frame. V^{GY} is the skew-symmetric matrix of the integrated velocity in the GY frame ($R_b^{GY} \cdot (R_b^e)^T \cdot v^e$).

Based on Equations (18), (19) and (20), the design matrix related to the GL/YRS velocity update is consequently shown in Equation (21).

$$\begin{aligned} z_{V_{GY}} &= v^{GY} - R_b^{GY} \cdot \left(R_b^e\right)^T \cdot v^e \\ &= -R_b^{GY} \cdot \left(R_b^e\right)^T \cdot N^e \cdot \Delta t \cdot \delta r^e + R_b^{GY} \cdot \left(R_b^e\right)^T \cdot \delta v^e \\ &\quad + \left[R_b^{GY} \cdot \left(R_b^e\right)^T \cdot V^E - R_b^{GY} \cdot \left(R_b^e\right)^T \cdot G^e \cdot \Delta t \cdot \right] \cdot \varepsilon^{b-e} \\ &\quad - M \cdot \Delta t \cdot \delta b_{GL} - J \cdot V_0^{GY} \cdot \Delta t \cdot \delta d_{Yaw} \\ &\quad + \left(G^{GY} \cdot \Delta t - V^{GY} \right) \cdot \varepsilon^{b-GY} \\ &= H_{V_{GY}} \cdot \delta x + w_{V_{GY}} \end{aligned} \quad (21)$$

where $H_{V_{GY}}$ is the design matrix for the GL/YRS update, which is coupled with the error states of position, velocity, b to e frame misalignment angles, GL/YRS biases as well as the misalignment angles between the b and GY frames.

Similarly, the WSS updates the centralized Kalman filter in the vehicle frame. The velocity in the integrated system is transformed from the e frame into the v frame. The measurement equation is expressed by Equation (22).

$$S \cdot V_{WSS} = R_b^v \cdot \left(R_b^e\right)^T \cdot v^e \quad (22)$$

where S is the WSS scale factor. V_{WSS} is the velocity used for the WSS update, which is given by Equations (12) to (14) in terms of the selected strategy.

In the same way as Equation (20), the perturbation of the right hand side of Equation (22) is analyzed in Equation (23).

$$\begin{aligned}\delta\left(R_b^v \cdot \left(R_b^e\right)^T \cdot v^e\right) &= R_b^v \cdot \left(R_b^e\right)^T \cdot \delta v^e \\ &+ R_b^v \cdot \left(R_b^e\right)^T \cdot V^E \cdot \varepsilon^{b-e} \\ &- V^V \cdot \varepsilon^{b-v}\end{aligned} \tag{23}$$

where V^E is the skew-symmetric matrix of the integrated velocity in the e frame. V^V is the skew-symmetric matrix of the integrated velocity in the v frame ($R_b^v \cdot \left(R_b^e\right)^T \cdot v^e$).

Therefore, the design matrix for the WSS can be derived from Equation (24)

$$\begin{aligned}Z_{WSS} &= S \cdot V_{WSS} - R_b^v \cdot \left(R_b^e\right)^T \cdot v^e \\ &= R_b^V \cdot \left(R_b^e\right)^T \cdot \delta v^e + R_b^v \cdot \left(R_b^e\right)^T \cdot V^E \cdot \varepsilon^{b-e} \\ &- V_{WSS} \cdot \delta S - V^V \cdot \varepsilon^{b-v} \\ &= H_{WSS} \cdot \delta x + \omega_{wss}\end{aligned} \tag{24}$$

where H_{WSS} is the design matrix for the WSS update, which is coupled with the error states of velocity, b to e frame misalignment angles, WSS scale factor, and the b to v frame misalignment angles.

The measurement noise or the measurement variance plays an important role in the integrated system. In this research, the measurement accuracy of the GL/YRS was determined from a static test by calculating the average standard deviation across 40 evenly spaced 1-second intervals of the static data. As the wheel speed sensor always output zero in static mode, its measurement accuracy was evaluated by means of NovAtel OEM2 precise velocity GPS receiver that measures the velocity at the millimeter per second level. The measurement accuracy of WSS and GL/YRS is summarized in Table 1.

Table 1: Measurement Accuracy of WSS and GL/YRS

WSS	0.05 m /s
GL1	0.065 m/s^2
GL2	0.071 m/s^2
YRS	0.408 deg/s

Based on measurement accuracy of the WSS and GL/YRS evaluated from a specially conducted test, the velocity variance for the GL/YRS and WSS update can be tuned adaptively in terms of variance propagation theory.

Equation (25) shows the variance of the specific forces in X and Y directions of GY frame derived from Equation (4) for GL1 and GL2.

$$\begin{cases}\sigma_{f_x}^2 = \left(\sigma_{GL1}^2 + \sigma_{GL2}^2\right)/2 \\ \sigma_{f_y}^2 = \left(\sigma_{GL1}^2 + \sigma_{GL2}^2\right)/2\end{cases} \tag{25}$$

where $\sigma_{f_x}^2$ is the variance of the specific force in the X direction of GY frame. $\sigma_{f_y}^2$ is the variance of the specific force in the Y direction of GY frame. σ_{GL1}^2 and σ_{GL2}^2 are the variances of the first and second G sensor that are evaluated from the static test.

From Equation **(16),** the measurement variance for the GL/YRS velocity update is shown in Equation (26)

$$\begin{aligned}\sigma_{V^{GY}}^2 &= \sigma_{V_0^{GY}}^2 + M \cdot \left(\sigma_f^2 + \sigma_{\delta b_{GL}}^2\right) \cdot M^T + J \cdot V^{GY}\left(\sigma_\gamma^2 + \sigma_{\delta d_{yaw}}^2\right) \\ &\cdot \left(J \cdot V^{GY}\right)^T + J \cdot \sigma_{V_0^{GY}}^2 \cdot \left(\gamma - d_{yaw}\right)^2 \cdot J^T\end{aligned} \tag{26}$$

where $\sigma_{V^{GY}}^2$ is the velocity variance of the GL/YRS in the GY frame. $\sigma_{\delta b_{GL}}^2$ and $\sigma_{\delta d_{Yaw}}^2$ are the estimated variance of the GL/YRS biases provided by the Kalman filter, and $\sigma_{V_0^{GY}}^2$ is the initial velocity variance that is related to the integrated velocity variance.

For a WSS update, the measurement accuracy in the Y direction of the vehicle frame equals the measurement accuracy of the wheel speed sensors if two non-holonomic constraints are used. However, if the lateral non-holonomic constraint is replaced by the lateral velocity computed from the GL/YRS, its variance is computed by taking into account Equations (10) and Equation (26), as shown in Equation (27)

$$\sigma_{V_{GY}^v}^2 = R_b^v \cdot \left(R_b^{GY}\right)^T \cdot \sigma_{V^{GY}}^2 \cdot R_b^{GY} \cdot \left(R_b^v\right)^T \tag{27}$$

In terms of Equation (11), the variance of the side slip angle is computed by Equation (28)

$$\begin{aligned}\sigma_{\beta_r}^2 &= \left[\frac{\partial \beta_r}{\partial (V_{GY}^v)_x}\right]^2 \cdot \sigma_{(V_{GY}^v)_x}^2 + \left[\frac{\partial \beta_r}{\partial (V_{GY}^v)_y}\right]^2 \cdot \sigma_{(V_{GY}^v)_y}^2 \\ &+ \left(\frac{\partial \beta_r}{\partial \gamma}\right)^2 \cdot \sigma_\gamma^2 = \frac{(V_{GY}^v)_y^2}{\left[\left((V_{GY}^v)_x - L_r \cdot \gamma\right)^2 + (V_{GY}^v)_y^2\right]^2} \bullet \\ &\left[\left(\frac{(V_{GY}^v)_x - L_r \cdot \gamma}{(V_{GY}^v)_y}\right)^2 \cdot \sigma_{(V_{GY}^v)_y}^2 + \sigma_{(V_{GY}^v)_x}^2 + L_r^2 \sigma_\gamma^2\right]\end{aligned} \tag{28}$$

where σ_r^2 is the measurement accuracy of the yaw rate sensor.

Using the variance of the side slip angle, the variance of the decomposed velocity can be calculated by Equation (29) .

$$\begin{cases} \sigma_{V_{WSS}^X}^2 = \sigma_{v_{wss}}^2 \sin^2(\beta_r) + v_{wss}^2 \cdot \cos^2(\beta_r) \cdot \sigma_{\beta_r}^2 \\ \sigma_{V_{WSS}^Y}^2 = \sigma_{v_{wss}}^2 \cos^2(\beta_r) + v_{wss}^2 \cdot \sin^2(\beta_r) \cdot \sigma_{\beta_r}^2 \end{cases} \quad (29)$$

where $\sigma_{v_{WSS}}^2$ is the measurement accuracy of the wheel speed sensor.

TEST DESCRIPTIONS, RESULTS AND ANALYSIS

A field test was conducted in an open sky area with good GPS availability. It covered typical vehicle dynamics such as constant velocity, acceleration, deceleration, stationary mode and turning as well as downhill and uphill sections. A GPS reference station was set up on a pillar with surveyed coordinates, and the reference GPS data was collected at 20 Hz by a NovAtel OEM4 GPS receiver. The HG1700 tactical grade IMU was time tagged by the NovAtel's Black Diamond System (BDS), and was sampled at 100 Hz. As a part of the BDS, one NovAtel OEM4 GPS receiver recorded data at 1 Hz to function as a rover. The WSS and GL/YRS were time tagged by another NovAtel OEM4 GPS receiver, and their data was logged to a desktop PC at 20 Hz.

To evaluate the effects of different integration strategies and algorithms, the reference trajectory was generated by the integration of GPS and the navigation grade CIMU. The GPS/CIMU integrated solution was processed by the PosPac software from the Applanix Corporation. With the optimally accurate and the backward smoothed solution, the horizontal accuracy of the reference trajectory is better than 1.4 cm.

Four GPS outages were simulated for the analysis of the horizontal positioning drift error with respect to four integration strategies, namely:

1. Strategy 1: GPS/INS integrated system. In this case, no aiding comes from the vehicle sensors. During GPS outages, the free-inertial system drifts with time without bounding.

2. Strategy 2: GPS/INS/GL/YRS/WSS integrated system with two non-holonomic constraints for the WSS update. In this strategy, the GL/YRS and WSS update the centralized Kalman filter sequentially, and the GL/YRS and WSS with two non-holonomic constraints are used to limit the free-inertial position drift during GPS outages.

3. Strategy 3: GPS/INS/GL/YRS/WSS with the lateral velocity. The difference of this strategy with the last one is that the lateral velocity calculated from the GL/YRS is applied to the WSS to remove the lateral non-holonomic constraint in Case 2.

4. Strategy 4: GPS/INS/GL/YRS/WSS with the rear wheel side slip angle. Similar to Strategy 3, this strategy reduces the lateral constraint by decomposing the WSS measurement through the side slip angle. The difference between this strategy and Strategy 3 is that this strategy uses the WSS measurement and the rear wheel side slip angle to calculate the lateral and longitudinal velocities for WSS update.

Among the four simulated GPS outages, two had larger side slip angles (The first one was at the maximum of 21 degrees, and the second one was at the maximum of 7 degrees), and the other two had relatively small side slip angles (The first one was less than 1 degree, and the second one was less than 2 degree). As the side slip angle has a direct relationship with the vehicle dynamics, the horizontal position drift errors of all integration strategies are analyzed with respect to both the side slip angle and the vehicle dynamics.

Figure 7 shows that the vehicle starts to move from a stationary position. The acceleration in the south direction and the changes in the roll and azimuth angles appear between 10 to 15 s. Consequently, a big side slip angle occurs within this time period as shown in Figure 8. In Figure 9, the blue line represents the GPS/INS integration strategy (Strategy 1), the red line GPS/INS/GL/YRS/WSS with non-holonomic constraints (Strategy 2), the green line GPS/INS/GL/YRS/WSS with the lateral velocity from GL/YRS replacing the lateral constraint (Strategy 3), and the black line represents GPS/INS/GL/YRS/WSS with the lateral and longitudinal velocities decomposed by the side slip angle (Strategy 4).

In general, external aiding from GL/YRS/WSS can significantly reduce the horizontal position error compared with the free inertial system. When the car operates in static mode, Strategies 2, 3 and 4 basically produce the same results. When the vehicle starts to move and before a larger side slip angle (The maximum side slip angle is about 21 degree) appears, Strategies 2 and 3 produce the basically same results, and the horizontal position drift error for Strategy 4 is larger than Strategies 2 and 3. The reason to account for this is that during static mode the vehicle is parked on a rough road which introduces relatively large pitch and roll angles. The rough road most likely produces a side slip angle. However, due to the small velocity within this time period, the side slip angle is not accurately calculated, which leads to a negative effect on Strategy 4. However, after a larger side slip angle occurs, both Strategies 3 and 4

(without a lateral non-holonomic constraint) outperforms Strategy 2 which contains a lateral non-holonomic constraint. It indicates that non-holonomic constraints are no longer valid when a larger side slip angle exists. Using the lateral velocity calculated from other independent sensors or decomposing the WSS measurement by the side slip angle can remove the lateral constraint, and consequently can improve the positioning accuracy. Due to the high inertia of the vehicle, the influence of a larger side slip angle on the system will last for some time. Therefore, the improvements on the positioning accuracy resulting from Strategies 3 and 4 will continue until the influence of the side slip angle vanishes.

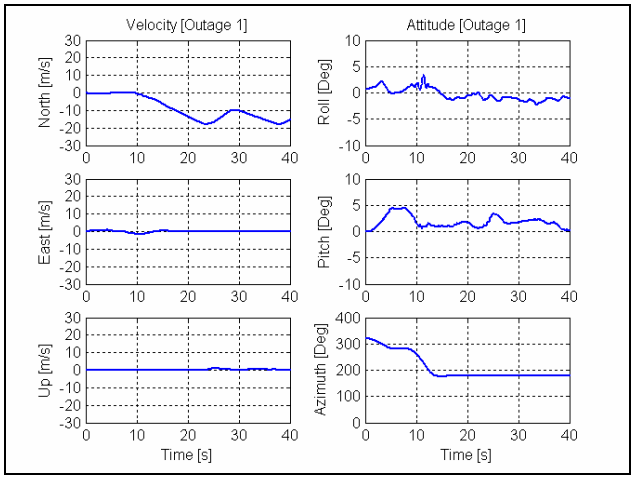

Figure 7: Vehicle Dynamics for GPS Outage 1

Figure 8: Side Slip Angle for GPS Outage 1

In Figure 10, the high vehicle dynamics between 20 s and 30 s, such as acceleration, deceleration, turning as well as the pitch and roll angle changes, lead to an maximum 7 degree side slip that can be seen in Figure 11.

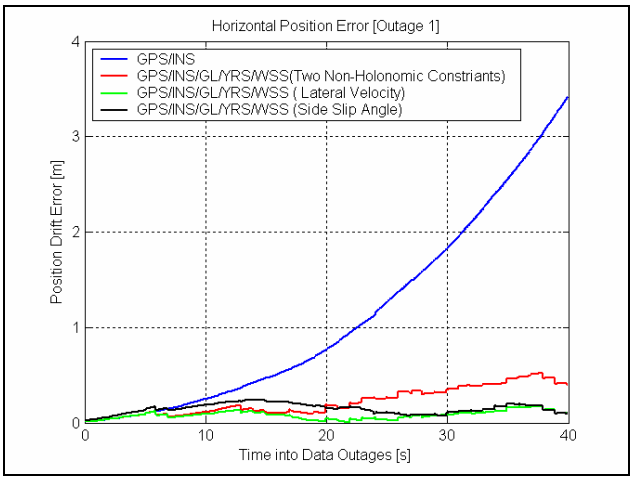

Figure 9: Horizontal Position Error for Outage 1

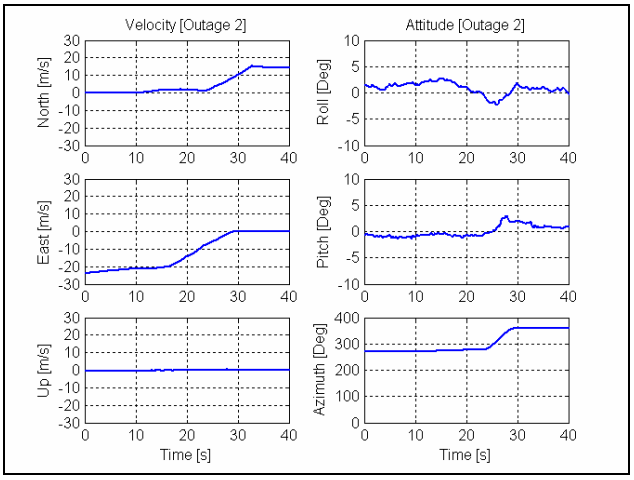

Figure 10: Vehicle Dynamics for GPS Outage 2

Figure 11: Side Slip Angle for GPS Outage 2

With respect to the horizontal position drift error in Figure 12, Strategies 2, 3 and 4 generate basically same

results with Strategy 2 being slightly better before the side slip appears. However, Strategies 3 and 4 outperform Strategy 2 after the side slip occurs all of a sudden, and their improvements will last for some time until the influences of the side slip on the system disappears. Comparing Strategies 3 and 4, Strategy 3 behaves better than Strategy 4 during the side slip, while their results are close to the same after the side slip. Since the wheel speed sensors are attached to the wheels, a larger side slip will definitely deteriorate the quality of the WSS measurement. This will in turn degrade the performance of Strategy 4, which decomposes the WSS measurement into lateral and longitudinal velocities by using the side slip angle. By contrast, GL/YRS measurements are less sensitive to side slip. Therefore during side slips, Strategy 4 is less robust than Strategy 3. But Strategy 4 still outperforms Strategy 2 by removing the lateral constraint violation during side slips.

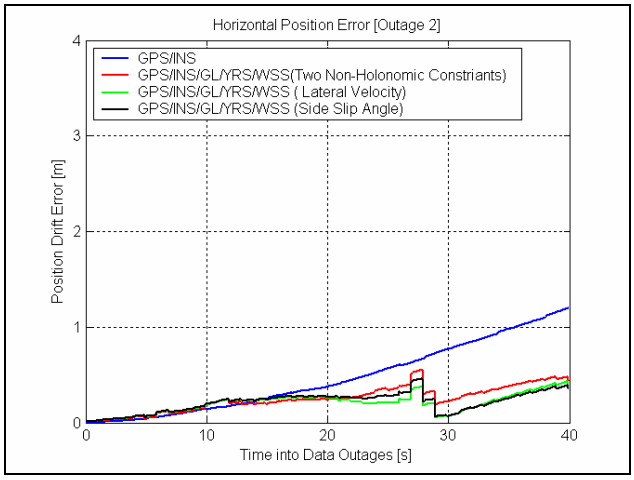

Figure 12: Horizontal Position Error for Outage 2

In GPS outage 3, as shown in Figure 13 and Figure 14, the vehicle runs westward without turning and large bumps, and the side slip angle is therefore very small. (The maximum side slip angle is about 1 degree). With the small side slip angle, the non-holonomic constraints are not violated. In Figure 15, the performance of Strategy 2 is better than Strategies 3 and 4. When the side slip angle is small, Strategy 2 with non-holonomic constraints is closer to the real situation. Strategies 3 and 4, however, still remove the lateral constraints using the lateral velocity or the WSS measurement decomposition, which will introduce more noise from the GL/YRS or WSS. It makes sense that when the side slip angle is small, no benefits can be expected from Strategies 3 or 4.

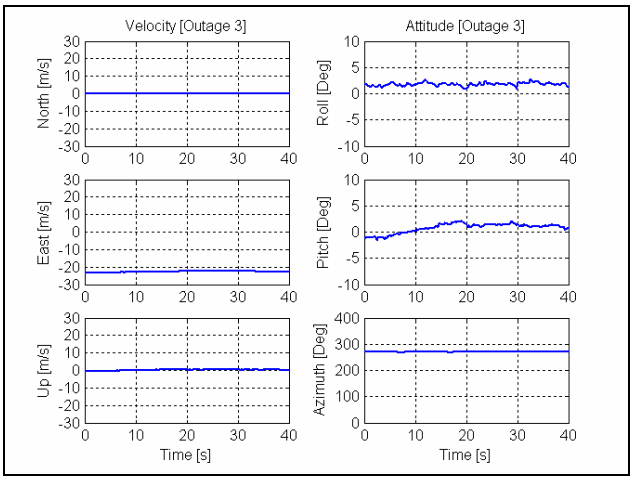

Figure 13: Vehicle Dynamics for GPS Outage 3

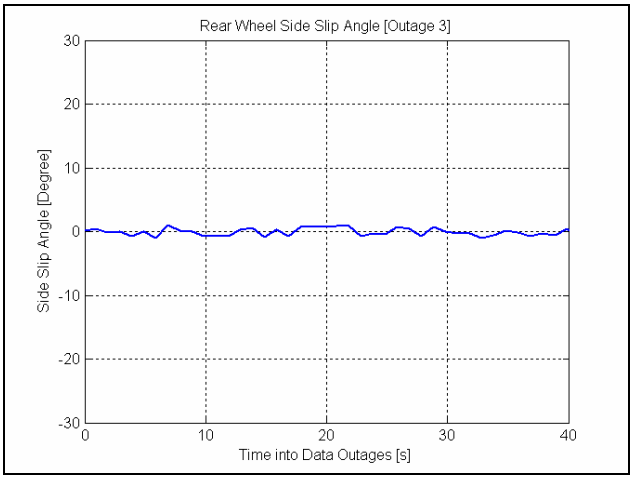

Figure 14: Side Slip Angle for GPS Outage 3

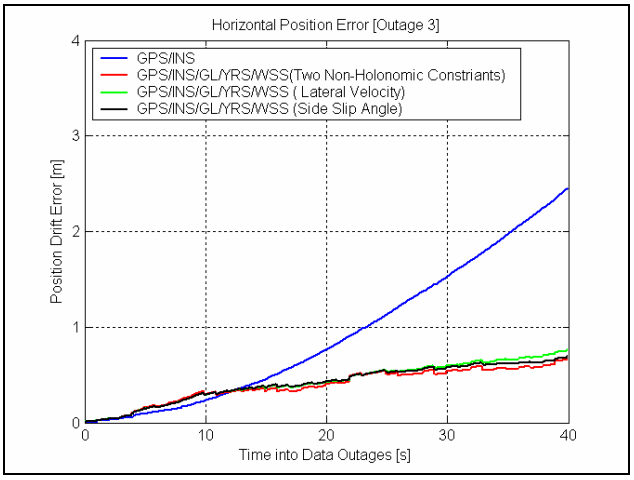

Figure 15: Horizontal Position Error for Outage 3

An extreme case can be seen from GPS outage 4. In Figure 16, the vehicle accelerates and decelerates

Northward in an intermittent way. Figure 17 shows that the side slip angle is very small (The maximum side slip angle is about 2 degree). It means that the non-holonomic constraints apply well in this scenario. It can be seen from Figure 18 that the horizontal position drift errors for Strategies 3 and 4 are larger than for Strategy 2. This is due to the fact that more noise is introduced into the system when computing the lateral velocity or side slip angle from GL/YRS when the non-holonomic constraints are not violated.

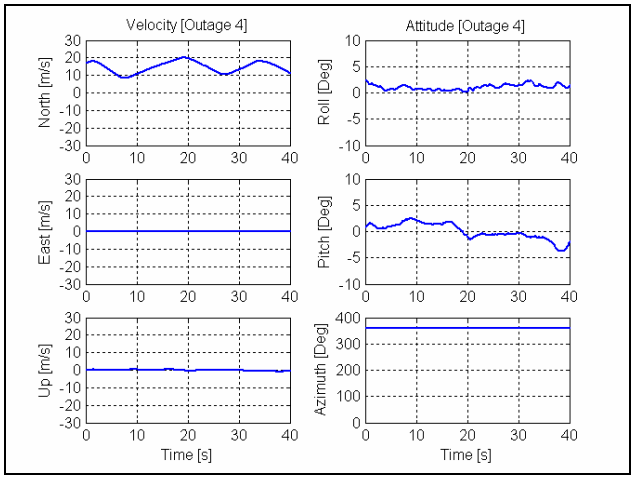

Figure 16: Vehicle Dynamics for GPS Outage 4

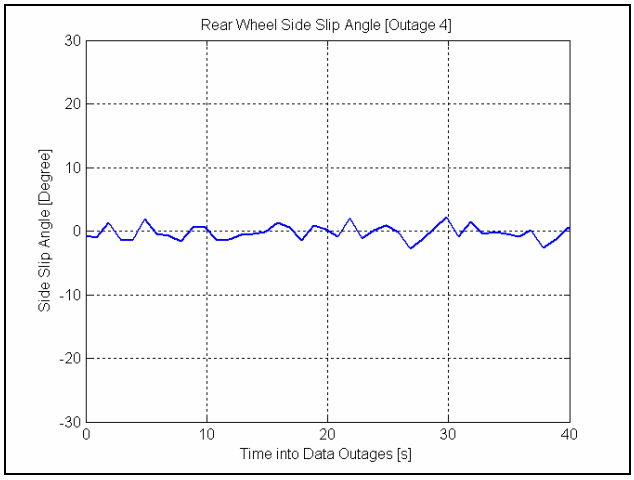

Figure 17: Side Slip Angle for GPS Outage 4

Table 2 summarizes the horizontal position errors for each strategy and each GPS outage. It also calculates the average of the horizontal position error and the average percentage improvement of Strategies 2, 3 and 4 over Strategy 1 on the horizontal position error. The non-holonomic constraints work better than any strategy that removes the lateral constraints when the side slip angle is small. When the side slip angle is larger, removing the non-holonomic constraints with the lateral velocity from the GL/YRS sensors is more robust than the WSS measurement decomposition with the side slip angle due to the fact that WSS measurements are sensitive to side slip.

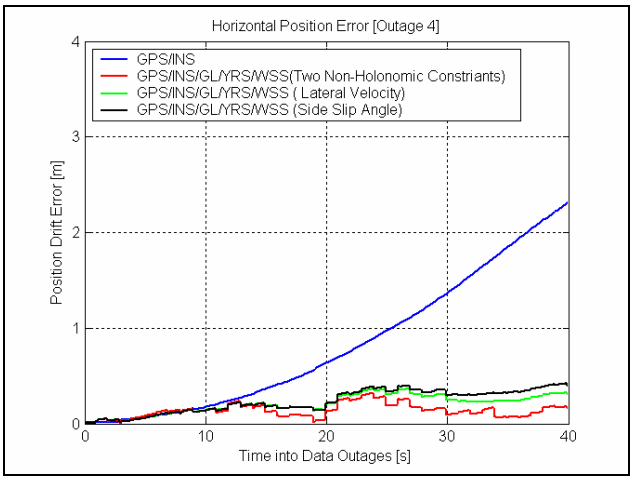

Figure 18: Horizontal Position Error for Outage 4

Table 2: Comparisons of Different Strategies

Outage	Horizontal Position Error at End of 40 s GPS Outages [m] Average Percentage Improvement over Strategy 1			
	Strategy 1	Strategy 2	Strategy 3	Strategy 4
1	3.42	0.40	0.09	0.10
2	1.20	0.45	0.40	0.36
3	2.46	0.68	0.76	0.70
4	2.32	0.16	0.30	0.40
Average	2.35	0.42	0.39	0.39
[%]	-	82.1	83.4	83.4

CONCLUSIONS

G sensors, yaw rate sensor, and wheel speed sensors are integrated with GPS/INS through a tight coupling strategy. When updating the Kalman filter by these sensors, a centralized Kalman filter can estimate the error states of wheel speed sensor scale factor, the G sensors and yaw rate sensor biases, the misalignement angles between different frames. The development of the integration algorithms includes the derivations of the equation of motion of G sensors and yaw rate sensor, the relationship between the on-board vehicle sensors, the dynamic and measurement equations used in the Kalman filter as well as the on-line tuning of the velocity variances for the velocity update. This was implemented in a vehicle positioning system and field tested under various conditions.

By creating an interactive relationship between the G sensors, yaw rate sensor and the wheel speed sensor, the

lateral velocity and the side slip angle can be computed to detect violations of non-holonomic constraints in the lateral direction. Two methods were tested to deal with this violation. The first was to use the computed lateral velocity to remove the lateral constraint. The second was to decompose the wheel speed sensor measurement into longitudinal and lateral velocities by using the side slip angle.

GPS outages were simulated to evaluate the horizontal positioning drift error by comparing four integration strategies. The results show that external aiding from the G sensor, yaw rate sensor and wheel speed sensor can significantly reduce the horizontal position error of the free inertial system. Non-holonomic constraints work better than any strategy that removes the lateral constraints when the side slip angle is less than 2 degrees. When the side slip angle is larger than 7 degrees, removing the non-holonomic constraints by the lateral velocity or by the decomposition of the wheel speed sensor measurement through the side slip angle outperforms the use of non-holonomic constraints. Removing the lateral constraint with lateral velocity is more robust than the strategy of decomposing the wheel speed sensor measurement with the side slip angle.

ACKNOWLEDGMENTS

The author would like to acknowledge his supervisor, Professor Elizabeth Cannon and Dr. Mark Petovello, Senior Research Engineer in the PLAN Group, for their support and suggestions on this research. This project was also partly supported financially by the AUTO 21 Network of Centres of Excellence.

REFERENCES

Anderson, R., Bevly, D.M. (2004). **Estimation of Slip Angles Using a Model Based Estimator and GPS.** Proceedings of the American Control Conference. Boston, Massachusetts, pp. 2122-2127, 2004.

Brandit, A. Gardner (1998). **Constrained Navigation Algorithms for Strapdown Inertial Navigation Systems with Reduced Set of Sensors.** Proceedings of the American Control Conference. Philadelphia, Pennsylvania. 1998.

Dissanayake, G., Sukkarieh, S., Nebot, E. and DurrantWhyte, H. (2001). **The aiding of a Low Cost Strapdown Inertial Measurement Unit suing Vehicle Model Constraints for Land vehicle Applications.** IEEE Transactions on Robotics and Automation, Vol.17, No. 5, 2001, pp. 731-747.

Gao, J., Petovello, M. and Cannon, M.E. **Development of Precise GPS/INS/Wheel Speed Sensor/Yaw Rate Sensor Integrtaed System.** Proceeding of ION NTM 2006, (January, Monterey, CA)

Harvey, R.S. (1998). **Development of a Precision pointing System Using an Integrated Multi-Sensor Approach**. M.Sc. thesis, UCGE Report, Department of Geomatics Engineering, University of Calgary.

Hay, C. (2005) **Turn, Turn, Turn Wheel-Speed Dead Reckoning for Vehicle Navigation**. GPS World, October, 2005, pp 37-42.

Jekli, C. (2000) **Inertial Navigation Systems with Geodetic Applications.** Walter de, Gruyter, New York, NY, USA.

Kubo, J., Kindo, T., Ito, A. and Sugimoto, S. (1999) **DGPS/INS/Wheel Sensor Integration for High Accuracy Land-Vehicle Positioning**. Proceedings of ION GPS 1999. (September, Nashville, TN), pp. 555-564.

Petovello, M.G. (2003) **Real-Time Integration of Tactical Grade IMU and GPS for High-Accuracy Positioning and Navigation.** PhD Thesis, UCGE Report #20116, Department of Geomatics Engineering, University of Calgary.

Ray, L.R. (1995). **Nonlinear State and Tire Force Estimation for Advanced Vehicle Control** IEEE Transactions on Control System Technology, Vol.3, No. 1, 1995, pp. 117-124.

Stephen, J. (2000). **Development of a Multi-Sensor GNSS Based Navigation system.** M.S.c. Thesis, UCGE Report, Department of Geomatics Engineering, University of Calgary

Sujit, S., Tomizuka, M. (1997). **Slip Angle Estimation for Vehicles On Automated Highways.** Proceedings of the American Control Conference. Albuquerque, New Mexico, 1997.